RSC Advances

PAPER

View Article Online
View Journal | View Issue

Cite this: *RSC Adv.*, 2024, **14**, 32239

Detection of mercury(II) in aqueous media using bodipy-functionalized magnetic fluorescent sporopollenin†

Melike Bayrak,[a] Aysel Cimen [a] and Ali Bilgic *[b]

Pollution from heavy metal ions has become a major issue worldwide. Water pollution, particularly with heavy metals like mercury, is a global problem. Developing environmentally friendly, low-cost, high-efficiency, sensitive, and selective sensors for the detection of mercury(II) ions in aqueous environments has attracted great interest in industry and academia. In this research paper, a bodipy-functionalized magnetic fluorescent **MSp-TAB** hybrid material was developed for detecting mercury(II) in aqueous media. The magnetic fluorescent **MSp-TAB** hybrid material was characterized using FT-IR, SEM, EDX, XRD, and TGA. We studied the influence of diverse factors such as contact time, temperature, and pH on the detection of Hg(II). The fluorometric study demonstrated that the developed magnetic-fluorescent hybrid material was sensitive/selective for Hg(II) ions in the absence and presence of interfering ions with a limit of detection (LOD) of 2.72 μM. In conclusion, the developed magnetic fluorescent **MSp-TAB** hybrid material has demonstrated its applicability and potential for accurate, sensitive, and practical detection of Hg(II) in tap water samples.

Received 4th September 2024
Accepted 2nd October 2024

DOI: 10.1039/d4ra06386d

rsc.li/rsc-advances

1. Introduction

The uncontrolled rapid development of technology and industry in our age has negative effects on the environment and society. These negativities create serious effects such as heavy metal ion pollution, especially on our ecosystems.[1–3] Heavy metal ions that cause water pollution in our ecosystem are harmful because water affects all life forms immediately.[4] In addition, the harmful effects of even trace amounts of heavy metals in aqueous masses are dangerous for human and ecosystem health.[5,6] For heavy metals, mercury, lead, chromium, cadmium, and arsenic are ranked as priority heavy metals potentially harmful to public health due to their high toxicity.[6] Among these heavy metals, mercury (Hg) is an important environmental pollutant due to its properties as a neurotoxic, teratogenic, mutagenic, and carcinogenic element with complex chemistry in the environment.[7–9] The main sources of mercury in the environment and other anthropogenic sources are oil refineries, petrochemical plants,[10] and businesses such as wastewater, hydrocarbon processing in gas plants, steel and iron factories, chlor–alkali industries, gold production, non-ferrous metal smelting, cement industries, coal, and fossil fuel combustion.[11,12] In general, mercury exists in three popular forms: organic mercury (CH_3Hg^+), elemental mercury (Hg^0), and inorganic mercury (Hg^{2+}).[12,13] Contamination by inorganic mercury compounds in these forms, especially mercury(II) derivatives, is a major hazard due to their highly toxic effects on humans.[14] It accumulates in human tissues and damages the kidneys, digestive system, stomach, liver, capillaries, lungs, and heart.[8,15–17] In addition, prolonged exposure to high levels of mercury can cause brain damage and death in humans.[18–22] For these reasons, it is necessary to develop simple, economical, environmentally friendly, and sensitive methods for the determination of inorganic mercury(II).

The conventional determination of inorganic mercury(II) is generally accomplished in specialized labs using electroanalytical techniques,[23] cold vapor atomic absorption spectrometry,[24] inductively coupled plasma atomic emission spectrometry,[25] atomic fluorescence spectrometry,[26] and inductively coupled plasma mass spectrometry.[14,27] These methods enable accurate identification of mercury(II) at trace levels,[14] but they are time-consuming, require complex sample determination steps, require specialized skilled operators and expensive equipment, and are generally not suitable for *in situ* detection of mercury(II).[28–31] Therefore, the development of simple, accurate, economical, sensitive, environmentally friendly, specific, convenient, and portable analytical methods for field monitoring of mercury(II) is of great interest.[14,31–33] Fluorescence-based chemosensors in particular are favoured for their unique features such as low cost, direct visual detection, high

[a]*Department of Chemistry, Kamil Ozdag Science Faculty, Karamanoglu Mehmetbey University, 70100, Karaman, Turkey*

[b]*Vocational School of Technical Sciences, Karamanoglu Mehmetbey University, 70100, Karaman, Turkey. E-mail: alibilgic100@hotmail.com; Fax: +90 338 226 21 66; Tel: +90 338 226 21 69*

† Electronic supplementary information (ESI) available. See DOI: https://doi.org/10.1039/d4ra06386d

sensitivity, and fast response.[34–37] In recent years, many fluorescent-based chemosensors have been developed for the sensitive/selective detection of Hg(II) ions.[37–43] Within fluorescence-based chemosensors, there's a rising trend in utilizing environmentally friendly hybrid materials. Sporopollenin, possessing such qualities, stands out as a natural and eco-friendly hybrid material. Studies on the successful removal and removal detectionof heavy metals using sporopollenin-based functional products are ongoing.[37,44–48] Sporopollenin (Sp) is called, the outer shell of plant pollen left over after the sporoplasm core is extracted, and is regarded as one of the most resistant biopolymers found in nature.[49–51] Sp has properties such as ideal grain size, regular structure, cross-linked, biological, chemical, physical properties, and thermal stability.[37,52,53] Although Sp biopolymers demonstrate excellent stability even after prolonged exposure to a wide range of organic and inorganic chemicals, the practical separation of Sp from water and solutions remains a significant challenge.[37,54] To solve this issue, sporopollenin can be readily functionalized and modified with iron oxide nanoparticles[55] due to the availability of a substantial internal cavity.[56,57] The incorporation of Fe_3O_4 into the Sp confers upon it the capacity to be readily separated from the solution environment using a magnetic field, obviating the necessity for the use of centrifugation and filtering processes.[37,58] Furthermore, the backbone of sporopollenin has oxygen, hydrogen, and carbon with branched and straight aliphatic chains[57,59] and its honeycomb-like structure makes it an effective host for interaction with different nanoparticles, adsorbates, and compounds.[57,60] The surface of the sporopollenin immobilized with fluorescent compounds can also be utilized for the efficient recognition of heavy metal ions. However, the idea of using magnetic fluorescent sporopollenin is rather limited in the literature.[37,61] Bodipy's are outstanding dyes among fluorescent compounds due to their great stability, strong quantum yield, sharp emission band, and ability to be seen with ultraviolet light and the naked eye.[47,62–64]

Based on the details provided in the preceding paragraphs, a new magnetic fluorescent **MSp-TAB** hybrid material has been created for the selective and sensitive detection of Hg(II) ions in aqueous settings. The fluorescent surface of the prepared hybrid material was systematically characterized by different techniques. The influence of pH, response time, and temperature on the detection of Hg(II) ions using magnetic fluorescent **MSp-TAB** hybrid material was also investigated. The prepared eco-friendly magnetic fluorescence hybrid material will guide and direct future research.

2. Experimental section

2.1. Materials used

All chemicals and materials utilized in the study were employed in their original state, without further purification, meeting analytical grade standards. $FeCl_3 \cdot 6H_2O$ (99%), dichloromethane (anhydrous, ≥99.8%), HNO_3 (ACS reagent, ≥90.0%), CH_3OH (≥99.9%), $(C_2H_5)_2O$ (≥99.0%), toluene (99.8%), NaOH (≥98%), HCl (37%), ethanol (99%), and ammonia (25%) were acquired from Merck (Darmstadt, Germany). 1-(4-Amino-2-hydroxyphenyl)ethan-1-one (AHAP) were purchased from Maybridge (England). Potassium dichromate, $AgNO_3$, $FeCl_2 \cdot 4H_2O$ (>99%), 2,4-dimethyl-3-ethylpyrrole, chloroform-d (99.8 atom % D), acetone, *N*-[3-(trimethoxysilyl)propyl]ethylenediamine (TPED, 97%), *Lycopodium clavatum* sporopollenin (particle size 25 μm), triethylamine (TEA, 99.5%), and 1,3,5-benzenetricarbonyl chloride were supplied from Sigma-Aldrich (Product of Germany). The cation solutions utilized in the sensor investigation were perchlorate salts procured from Merck (Darmstadt, Germany). The devices used are given in the ESI.†

2.2. Synthesis of magnetic sporopollenin (MSp)

The synthesis approach for magnetic sporopollenin (MSp) was conducted in a manner akin to the prior method.[54,65] In summary: 3.05 g of $FeCl_3 \cdot 6H_2O$ and 1.12 g of $FeCl_2 \cdot 4H_2O$ salts were added to the 0.25 L reaction vessel, and then 100 mL of purified water was supplemented into this reaction vessel. The salts present in the resulting solution underwent sonication for 10 minutes to ensure their complete dissolution. After complete dissolution, Sp (1.0 g) was added to this reaction vessel and stirred for 30 min under laboratory conditions, and 5 mL of NH_4OH (28%) was added and mixed again at 550 rpm for another 30 min at 90 °C. After mixing was finished, it was left to cool, and the MSp obtained was collected using a magnet and washed with plenty of water. This procedure was applied 3 times. The formed magnetic sporopollenins (MSp) were kept in an oven at 70 °C until they were modified with TPED. A schematic representation of the possible structure of the prepared MSp is shown in Fig. 1.

2.3. Preparation of magnetic MSp-T

All of the resulting MSp and 4.8 mL of TPED compound were supplemented into a 0.1 L reaction vessel containing acetonitrile (0.05 L). The mixture was subjected to continuous stirring and refluxed for a duration of 72 hours. Following the completion of the reaction time, the mixture was allowed to cool for 2 hours, after which **MSp-T** was retrieved using a magnet. The **MSp-T** was thoroughly washed with CH_3OH (30 mL), H_2O water (50 mL), and finally C_2H_5OH (30 mL), and then kept in an oven at 70 °C until its reaction with the AHAP compound. A schematic representation of the possible structure of the prepared **MSp-T** is demonstrated in Fig. 1.

2.4. Preparation of magnetic MSp-TA

All of the obtained by the above method and 0.5 g of AHAP compound were supplemented into a 0.1 L reaction vessel containing acetonitrile (0.05 L). This resulting suspension solution was refluxed for 72 h. Once the reaction reached completion, it was permitted to cool down, and the resulting product, **MSp-TA**, was extracted from the reaction vessel using a magnet. The obtained product (**MSp-TA**) underwent thorough washing with CH_3OH (50 mL), distilled H_2O (50 mL), and finally C_2H_5OH (20 mL). Subsequently, it was placed in an oven at 70 °C, awaiting its reaction with the bodipy dye. A schematic representation of the possible structure of the prepared **MSp-TA** is demonstrated in Fig. 1.

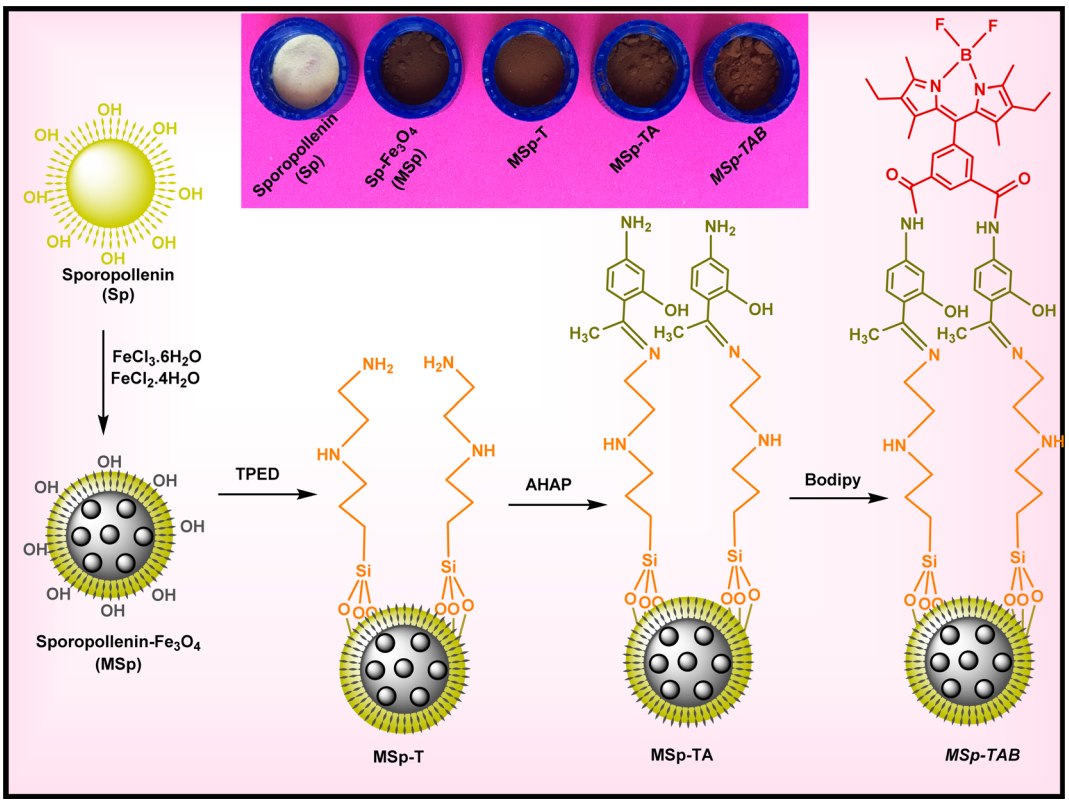

Fig. 1 Visual representations in a schematic format of Sp, MSp, **MSp-T**, **MSp-TA**, and **MSp-TAB**.

2.5. Preparation of magnetic fluorescent MSp-TAB hybrid material

The synthesis procedure of the fluorescent bodipy compound used in the study was carried out and characterized as in our previous studies.[66–68] To synthesize magnetic fluorescent **MSp-TAB** hybrid material, firstly, all of the **MSp-TA** obtained was supplemented into a 0.1 L reaction vessel containing 50 mL of acetonitrile, and then 0.2 g of bodipy dye was added to this reaction mixture. The mixture underwent refluxing for a duration of 72 hours. Once the reaction concluded, it was cooled, and the resultant magnetic-fluorescent hybrid material was extracted from the reaction vessel using a magnet. The resulting product (magnetic fluorescent **MSp-TAB** hybrid material) was thoroughly washed with CH_3OH, distilled H_2O, and C_2H_5OH. A schematic representation of the possible structure of the magnetic fluorescent **MSp-TAB** hybrid material is shown in Fig. 1.

2.6. Metal ion recognition and reuses studies

For studies of the detection of cation, firstly, 0.15 g L^{-1} of the as-prepared magnetic fluorescent **MSp-TAB** hybrid material was added to 250 mL beakers containing 100 mL EtOH/H_2O (30/70: v/v). The resulting suspension was sonicated for 15 min to ensure homogeneous dispersion of the magnetic fluorescent **MSp-TAB** hybrid material in the suspension mixture. Except for Ag(I) ($AgNO_3$) and Cr(VI) $K_2Cr_2O_7$, standard solutions of 1×10^{-2} M were prepared from the perchlorate salt of the cation ions. The cation solution (1×10^{-4} M, 0.3 mL) was poured into a centrifuge tube containing the magnetic fluorescent hybrid material solution (2.7 mL). The resulting suspensions were mixed for 60 minutes. Three repeated spectra were obtained at room temperature using a fluorescence spectrometer. Emission spectra were measured over the wavelength range 460–650 nm under 350 nm excitation.

3. Results and discussions

3.1. Characterizations

3.1.1. FT-IR analysis. Measurements were made with FT-IR spectroscopy to reveal the functional groups in the structure of the Sp, MSp, **MSp-T**, **MSp-TA**, and the magnetic fluorescent **MSp-TAB** hybrid material. FT-IR spectra of the Sp, MSp, **MSp-T**, **MSp-TA**, and the magnetic fluorescent **MSp-TAB** hybrid material are given in Fig. 2a–e comparatively. The FT-IR spectrum (Fig. 2a) of sporopollenin demonstrated all the characteristic peaks occurring at 3382 cm^{-1} (the stretching vibrations of hydroxyl (O–H)), 2925–2855 cm^{-1} (the stretching vibrations of saturated carbons (C–H)), 1708 cm^{-1} (the stretching vibrations of carbonyl (C=O) groups), and 1440 cm^{-1} (the bending vibration of C–H).[44–46,53,69] In the FT-IR spectrum of magnetic sporopollenin (MSp) (Fig. 2b), the new absorption peak at 560 cm^{-1} represents the stretching vibration of the Fe–O bond. The FT-IR spectrum of **MSp-T** obtained from the modification of TPED compound on the MSp surface is shown in Fig. 2c and the new peak at 1648 cm^{-1} (N–H) represents amine groups. In

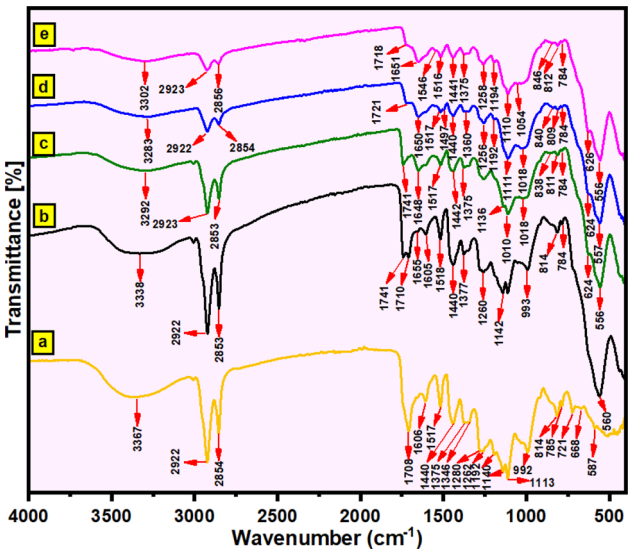

Fig. 2 The FT-IR spectra of (a) the Sp, (b) MSp, (c) **MSp-T**, (d) **MSp-TA** and (e) the magnetic fluorescent **MSp-TAB** hybrid material.

addition, Si–O and C–N stretching vibrations are observed at 1018 cm^{-1} and 1256 cm^{-1}, respectively (Fig. 2c). In the FT-IR spectrum of **MSp-TA** (binding of AHAP compound to the **MSp-T** surface) shown in Fig. 2d, the C=N stretching vibration represents the absorption peak at 1721 cm^{-1}. The absorption peak (Fig. 2d) at 1517 cm^{-1} represents the aromatic stretching (C=C) groups. In the FT-IR spectra of the magnetic fluorescent **MSp-TAB** hybrid material (Fig. 2e), the new peaks at 2923–2856 cm^{-1} (the aliphatic CH stretching), 1546 cm^{-1} (aromatic C=C bending), 1516 cm^{-1} (aromatic C=C stretching), and 1375 cm^{-1} (C–N stretching vibrations) represent. In addition, it represents Si–O–Si stretching (peaks at 1110 cm^{-1} and 1054 cm^{-1}) and Fe–O bending vibrations (peaks at 626 cm^{-1} and 556 cm^{-1}) (Fig. 2e). Apart from the spectral alterations mentioned earlier, the successful synthesis of the intended magnetic fluorescent **MSp-TAB** hybrid material is affirmed by variations in the intensity of additional characteristic peaks, peak shifts, and the appearance of newly formed peaks, as depicted in Fig. 2e.

3.1.2. XRD analysis. XRD analyses were conducted to assess the crystallinity of pure sporopollenin (Sp), MSp, **MSp-T**, **MSp-TA**, and the magnetic fluorescent **MSp-TAB** hybrid material. The XRD patterns for these materials, spanning the range of $2\theta = 10°$ to 80°, are presented in Fig. 3a–e. The XRD pattern of pure sporopollenin (Sp) in Fig. 3a exhibits, as in previous studies,[43,70] the broad diffraction peak at about 20° typically

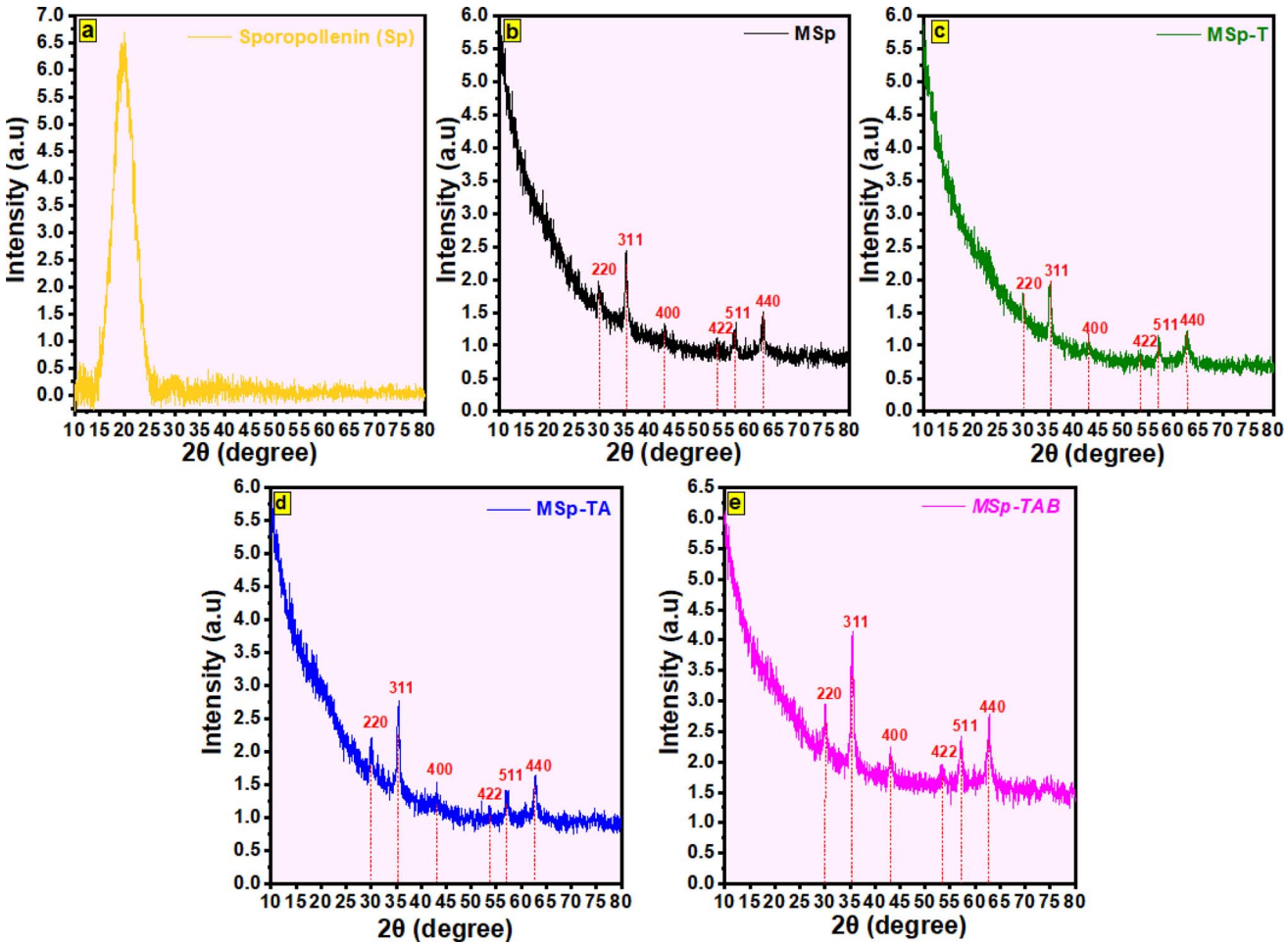

Fig. 3 XRD patterns of (a) Sp, (b) MSp, (c) **MSp-T**, (d) **MSp-TA** and (e) the magnetic fluorescent **MSp-TAB** hybrid material.

observed for amorphous material. Following the magnetization of the Sp surface with Fe_3O_4, the intensity of the diffraction peaks of Sp decreased and shifted approximately 10° in the XRD diffractogram of MSp (Fig. 3b). Several diffraction peaks for Fe_3O_4 nanoparticles were recognized in the XRD pattern of MSP in JCPDS card: 19-0629 data (2θ = 30.03° (220), 35.71° (311), 42.73° (400), 53.41° (422), 57.11° (511) and 62.51° (440)).[37,43,54,70] As seen in the XRD pattern of **MSp-T** materials (Fig. 3c) formed after modification of the MSp surface with TPED, a low diffraction peak at 20° to 25° represents the binding of the TPED compound (SiO_2) to the MSp surface.[37] On the other hand, in the X-ray diffraction diagrams of the magnetic materials formed after the binding of AHAP and Bodipy compounds to the **MSp-T** surface (Fig. 3d and e), there is no obvious difference other than the decrease/increase and shift in the intensity of the peaks, which indicates that the XRD crystal structures of MSp are preserved.

3.1.3. TGA analysis. The thermal stability of the materials prepared at each stage and the magnetic fluorescent **MSp-TAB** hybrid material was investigated by TGA analysis, and the TGA results at 20–700 °C at a thermal rate of 10 °C min^{-1} are shown in Fig. 4a–e. During the first stage of thermal degradation, occurring between 30 °C and 200 °C as depicted in Fig. 4a–e, weight loss was observed in all materials. This occurrence can be attributed to the elimination of volatile oxygen-containing functional groups like COOH, OH, CO, and water vapors from the materials, resulting from the breakdown of oxygenated functional groups.[71] The weight loss of materials in this range is approximately 3–4%. The mass loss of pure sporopollenin (Sp) in the range of 200–600 °C in Fig. 4a is due to the decomposition of the organic matter of Sp.[72] The weight loss in this temperature range (200–600 °C in Fig. 4a) is approximately 84.5%. The weight loss of the magnetic sporopollenin (MSp) in Fig. 4b at about 200–650 °C is attributed to the decomposition of organic materials.[72,73] The weight loss in this temperature range is approximately 64%. Above 650 °C the weight loss corresponds to the decomposition of magnetic nanoparticles.[73] The weight loss in the 200 to 500 °C range in Fig. 4c can be attributed to the dissociation of silica and aminopropyl groups in the TPED compound bound to the MSp surface.[71,74] On the other hand, the mass loss of the magnetic materials in the range of 200–600 °C in Fig. 4d and e can be attributed to the decomposition of silica and aminopropyl groups, AHAP and bodipy compounds. The weight losses in this temperature range (200–600 °C) are approximately 47% (Fig. 4d) and 47% (Fig. 4e), respectively.

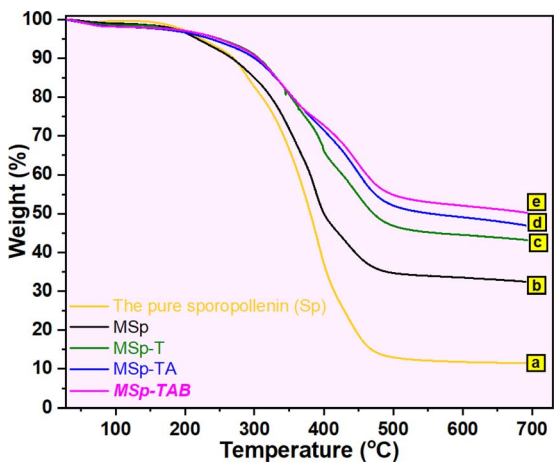

Fig. 4 TGA plots for (a) the Sp, (b) MSp, (c) MSp-T, (d) MSp-TA and (e) the magnetic fluorescent MSp-TAB hybrid material.

3.1.4. SEM and EDX analysis. Each stage was investigated by SEM, which is widely used to study the morphology of the prepared materials and magnetic fluorescence **MSp-TAB** hybrid material and SEM images of each material obtained from 100 μm to 10 μm are given in Fig. 5a–e. Fig. 5a depicts the morphology, demonstrating that the Sp microcapsules' surfaces have a smooth, porous structure and a regular hexagonal interconnected configuration. The MSp image in Fig. 5b shows that magnetic nanoparticles (Fe_3O_4) accumulate predominantly within the open pores of Sp and on the pore walls.[43,56,71] The SEM image of **MSp-T** in Fig. 5c demonstrates that the surface voids of MSp were filled with TPED after modification and became rougher. When the SEM image of **MSp-TA** in Fig. 5d is compared with the SEM image of **MSp-T** in Fig. 5c, the SEM image of **MSp-TA** in Fig. 5d appears to have a rougher porous structure and an irregular hexagonal structure. This confirms that the AHAP compound binds to the **MSp-T** surface. As shown in the SEM image of the magnetic fluorescent **MSp-TAB** hybrid material formed after immobilizing onto the magnetic **MSp-TA** material surface with bodipy (Fig. 5e), the uniform pore structure was disrupted and became rougher. SEM images and these explanations show that the sporopollenin structure maintains its morphology after functionalization (Fig. 5a–e).

The elemental compositions of the samples prepared at each stage were determined *via* EDX, and the obtained EDX results are given in Fig. 6a–e. The main element compositions of the prepared samples in Fig. 6a–e, as seen in the atomic and weight percentage data, confirm that the materials prepared at each stage were successfully prepared. Moreover, the energy dispersive X-ray (EDX) mapping for different elements (C, N, O, F, Si, and Fe) on the prepared magnetic fluorescent **MSp-TAB** hybrid material in Fig. 7 confirms the successful preparation of the **MSp-TAB**.

3.2. Metal ion detection studies

3.2.1. The response and selectivity of the magnetic fluorescent MSp-TAB hybrid material to several cation ions. Fluorescence variations in the spectrum were utilized to assess the potential metal recognition behavior of the newly synthesized magnetic fluorescent **MSp-TAB** hybrid materials. 2.7 mL (in 0.15 g per L ethyl alcohol/water (3/7)) of magnetic fluorescent **MSp-TAB** hybrid materials and 0.3 mL of different cations (1×10^{-4} M) were combined under laboratory conditions for the recognition investigation, and changes in fluorescence intensity (**MSp-TAB** and **MSp-TAB** + cations after 120 min) were noted. Fig. 8a shows a maximum fluorescence emission band at approximately 512 nm for the resulting magnetic fluorescent **MSp-TAB** hybrid material suspension mixture. Among the

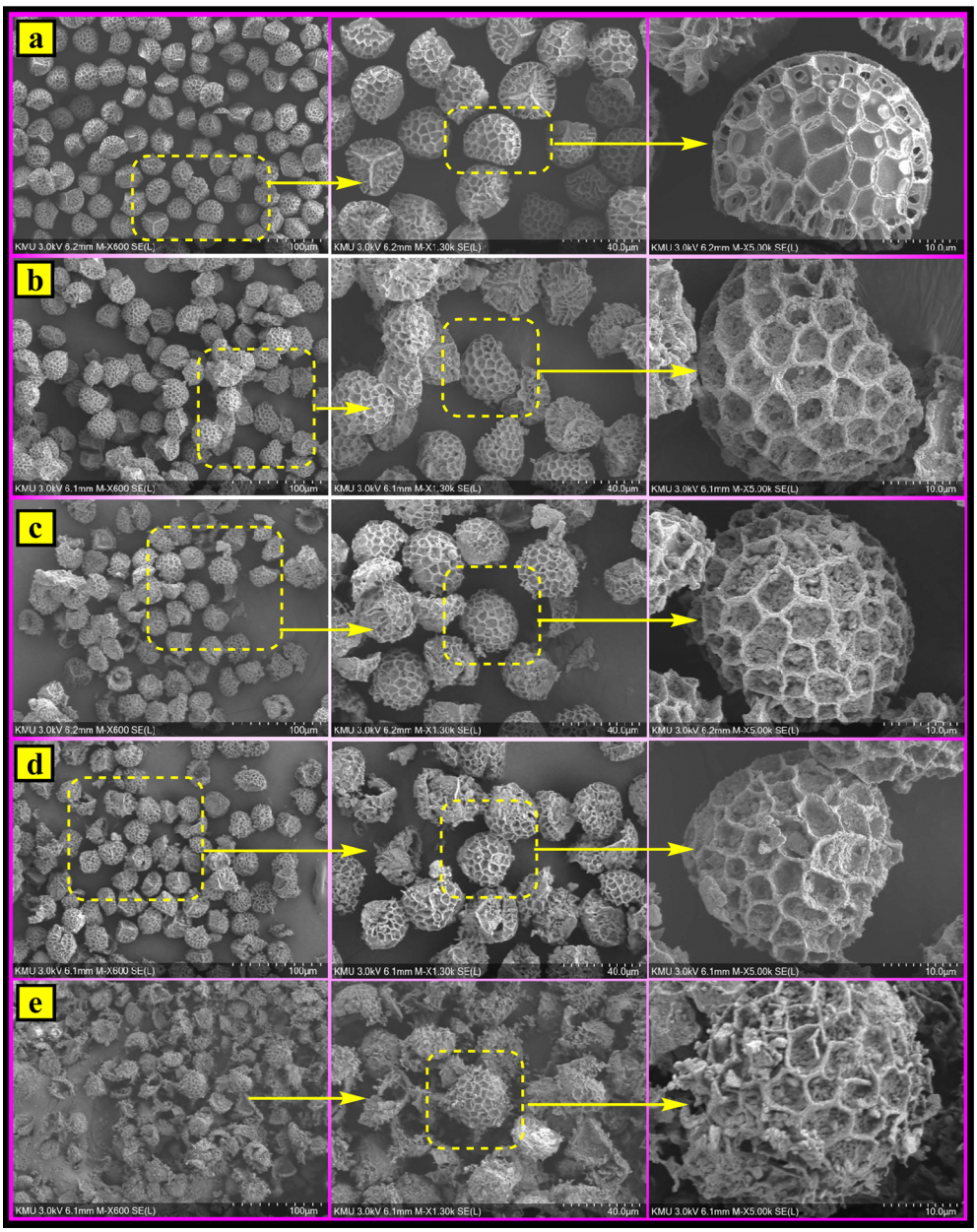

Fig. 5 SEM images for (a) the Sp, (b) MSp, (c) **MSp-T**, (d) **MSp-TA** and (e) the magnetic fluorescent **MSp-TAB** hybrid material.

tested cations, only Hg(II) induced alterations in the fluorescence spectrum of the magnetic fluorescent **MSp-TAB** hybrid (Fig. 8a). Upon addition of mercury(II) to suspension solutions of **MSp-TAB**, the emission maximum shifted from 512 nm to 523 nm ($\Delta\lambda \sim 11$ nm), accompanied by a 69% reduction in fluorescence intensity. Furthermore, a comparison was made of the photographic fluorescence detection properties of **MSp-TAB** suspensions spiked with metal ions using daylight and UV light. The quenching observed in the suspension mixture of the magnetic fluorescent **MSp-TAB** hybrid with Hg(II) demonstrates its outstanding selectivity for detecting this metal ion in water (Fig. S1†). Based on these observations, it can be inferred that **MSp-TAB** is well-suited for the fluorometric detection of mercury(II) ions.

The selectivity of the produced magnetic fluorescent **MSp-TAB** hybrid material for Hg(II) was confirmed by the addition of other cations (cations in Fig. 8b) at twice the concentration. The suspension samples (**MSp-TAB** + cation and **MSp-TAB** + cation + Hg(II)) were allowed to equilibrate for 120 min and fluorescence spectra were recorded. The fluorescence intensities obtained from the fluorescence spectra in the range of 512 nm and 523 nm are given as a column graph in Fig. 8b. As shown in Fig. 8b, there was no interference in the detection of Hg(II). Consequently, the presence of cations does not influence the fluorescence detection system, thus affirming **MSp-TAB**'s potential as a selective fluorescence sensor for Hg(II). After the addition of Hg(II), the wavelength was found to shift from 512 nm to 523 nm. The findings indicated that the presence of competitive cations did not notably impact the detection of

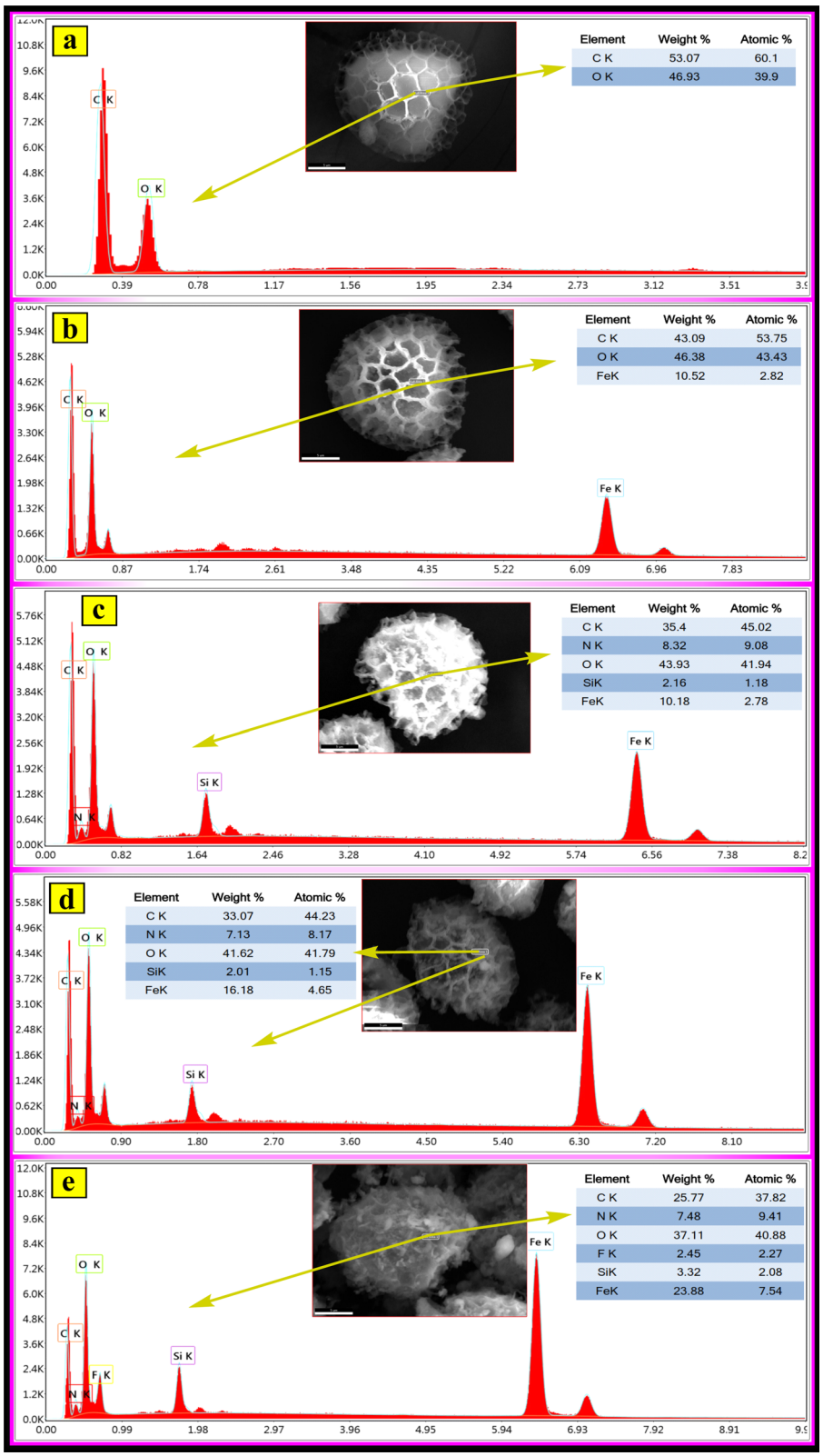

Fig. 6 EDX results of (a) the Sp, (b) MSp, (c) **MSp-T**, (d) **MSp-TA** and (e) the magnetic fluorescent **MSp-TAB** hybrid material.

Hg(II) by **MSp-TAB**. The excellent selectivity of **MSp-TAB** for Hg(II) and the lack of interference from other cations were the main findings of the fluorescence competition cation studies. This selectivity can be attributed to the intricate interactions between mercury(II) ions and the multi-amino groups and hydroxyl units present on the magnetic fluorescent **MSp-TAB**

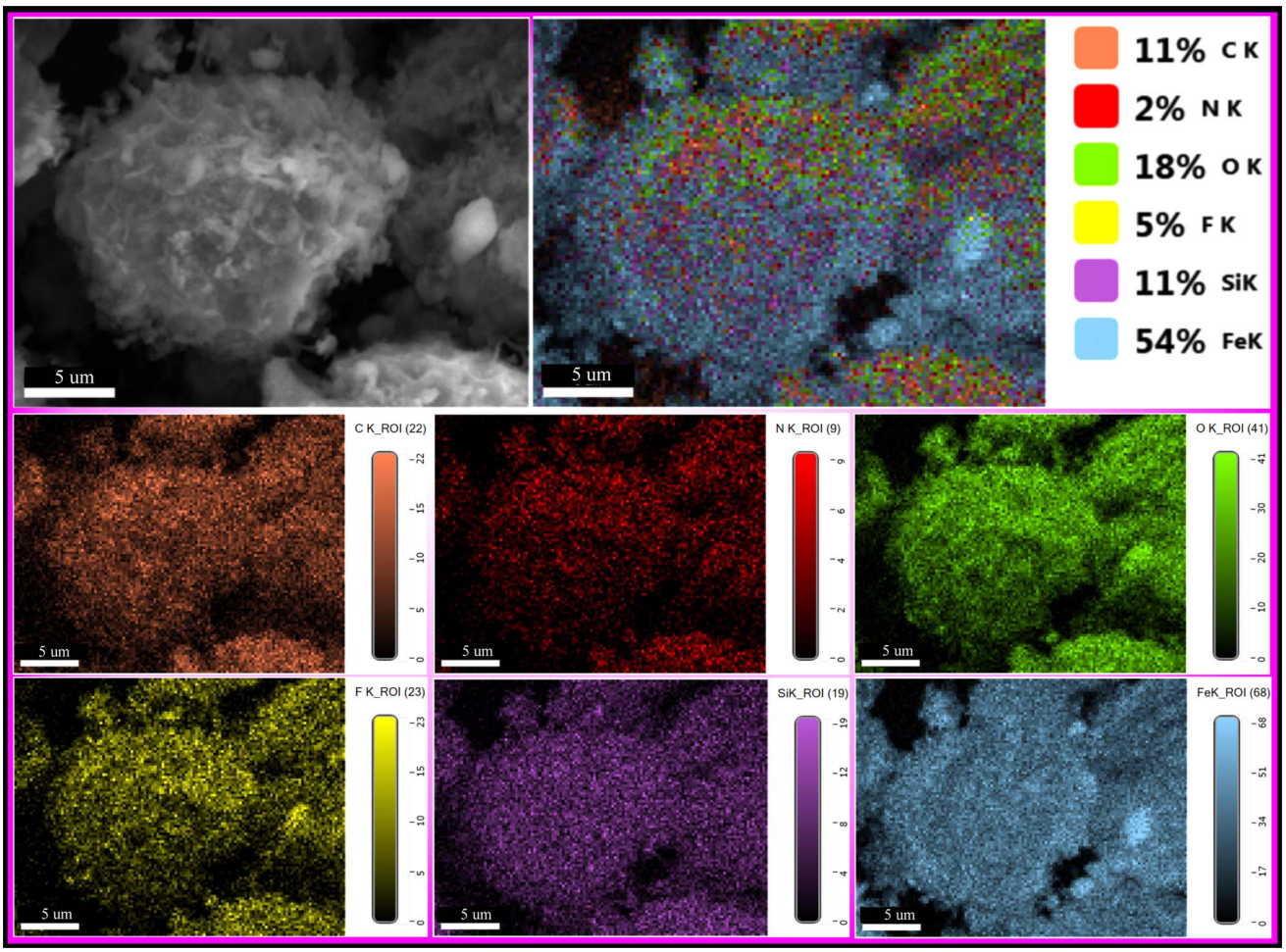

Fig. 7 SEM image with energy-dispersive X-ray (EDX) mapping for different elements (C, N, O, F, Si and Fe) on the magnetic fluorescent **MSp-TAB** hybrid material.

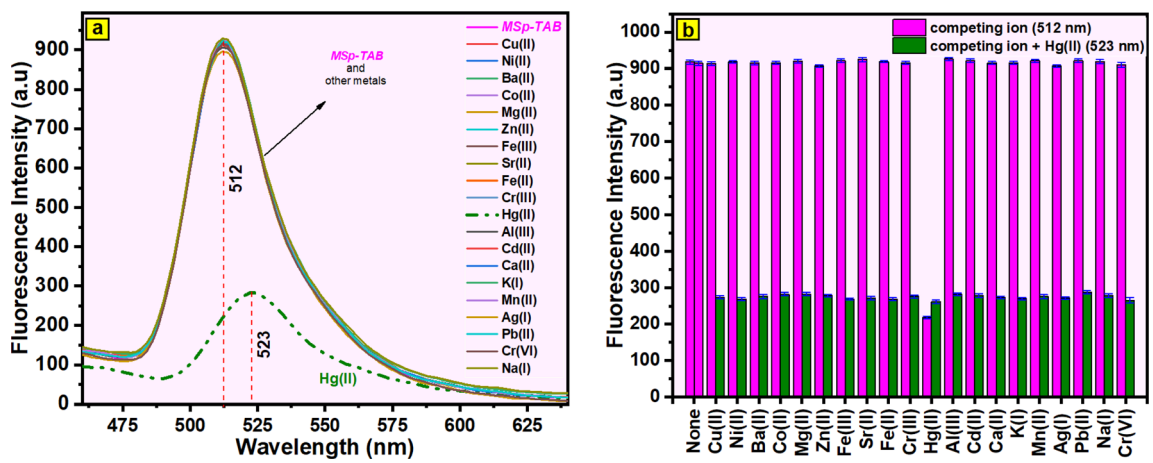

Fig. 8 (a) Fluorescence emission spectra (460–650 nm) of the magnetic fluorescent **MSp-TAB** hybrid material (0.15 g L^{-1} in ethyl alcohol/water (3/7)) after the addition of different cations. (b) Emission intensity changes at 512 nm and 523 nm of the magnetic fluorescent **MSp-TAB** hybrid material (0.15 g L^{-1} in ethyl alcohol/water (3/7)) in the presence of other metals with/without Hg(II). (Error analysis has been marked with error bars).

hybrid material surface. Both the donor atom cage enhances electron donation, and its diameter is well-suited for effectively binding mercury(II) ions.

3.2.2. Other selectivity studies. The influence of pH on the **MSp-TAB** and **MSp-TAB** + Hg(II) mixtures was examined at dissimilar pH values (1.0–10.0). The results obtained are given in Fig. S2a† in the form of a column plot of the influence effect of pH against fluorescence intensity. No obvious increase in the **MSp-TAB** suspension's fluorescence intensity was observed at different pH values, as shown in Fig. S2a.† The **MSp-TAB** + Hg(II) fluorescence intensity was lowest between pH 1.0 and 7.0 at 523 nm (Fig. S2a†), afterward, it is seen that the fluorescence intensity increases in the basic environment, that is, in the pH range 8.0–10.0', as shown in Fig. S2a.† This increase in fluorescence intensity suggests that the Hg(II) ion may hydrolyze to its hydroxide form and cannot form a complex with **MSp-TAB**. As a result, it was shown that the prepared **MSp-TAB** has good binding capacity to Hg(II) ions under acidic pH conditions.

The fluorescence response of suspension mixtures of **MSp-TAB** and Hg(II) + **MSp-TAB** (in H_2O/C_2H_5OH (3/7)) at dissimilar temperatures (15 °C, 25 °C, 35 °C, and 45 °C) was researched, and the results obtained are given in Fig. S2b† (512–523 nm). The cation-free **MSp-TAB** suspension (bright neon pink (512 nm)) in Fig. S2b† shows that temperature does not affect fluorescence intensity. After the addition of mercury cation, the 523 nm fluorescence intensities of **MSp-TAB** + Hg(II) suspension mixtures (Fig. S2b† green color) show that the fluorescence intensity decreases with increasing temperature. Based on these results, the decline in fluorescence intensity as temperature rises could be attributed to the expedited complexation of Hg(II) ions with the generated magnetic fluorescent **MSp-TAB** hybrid material.

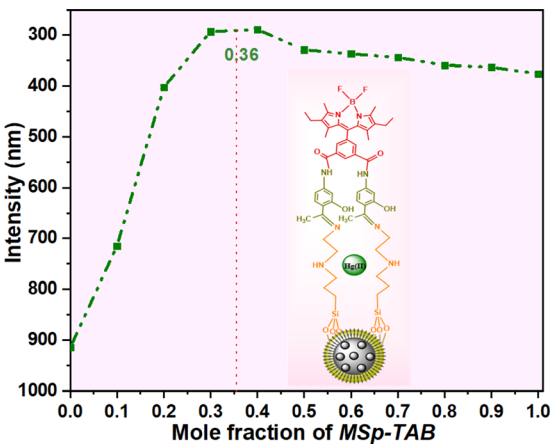

Fig. 9 Job's plot of the MSp-TAB + Hg(II) complex in a ethanol/water: (3/7).

The reaction time against mercury(II) cations was also examined for the prepared magnetic fluorescent **MSp-TAB** hybrid material. Changes in fluorescence intensity were monitored between 512 nm and 523 nm to determine **MSp-TAB** and **MSp-TAB** + Hg(II) response times (1–180 min). The results obtained are given in Fig. S2c.† The results showed no change in the fluorescence emission of the **MSp-TAB** suspension (bright neon pink colour (512 nm) in Fig. S2c†). On the other hand, it showed that the interaction between **MSp-TAB** and Hg(II) was completed in 25 min. After this minute, no difference in fluorescence intensity was observed.

3.2.3. Binding stoichiometry and limit of detection. To understand the binding stoichiometry between the Hg(II) cation and **MSp-TAB**, Job's plot experiments were performed using the emission intensities at 523 nm. The complex stoichiometry between **MSp-TAB** and Hg(II) (523 nm) indicates a 2 : 1 (ligand : metal) ratio, with a maximum value of 0.32 on the Job's plot graph (Fig. 9).

When Hg(II) cation (5–100 μM) was added to the magnetic fluorescent **MSp-TAB** hybrid detection system, the fluorescence intensity at 523 nm gradually decreased. It was investigated with the commonly used Limit of Detection (LOD) and the equation LOD = $3S_1/S$ was used.[66,67] Similar to prior research,[37] the standard deviation of blank measurements was determined by conducting 30 fluorescence spectrum measurements of **MSp-**

Table 1 Comparison of magnetic fluorescent MSp-TAB hybrid material with other reported methods and materials for Hg(II) detection

Probe	Technique	Linear range (μM)	LOD (μM)	Ref.
CA–AA–DTZ membrane	Colorimetric	15–50	15	75
Thiophene based Schiff base	Fluorimetry	—	20	76
A thio-urea based chromogenic and fluorogenic chemosensor	Fluorimetry and colorimetry	10–100	11.14	77
N–GQDs	Fluorimetry	20–100	0.42	78
Rhodamine–glyoxylic acid	Fluorimetry	5–200	1.0	79
N,S/C dots	Fluorimetry	0–40	2.0	80
Chlorophyll functional Ag NPs	Colorimetry	0.1–200	2.7	81
Probe JUTH	Fluorimetry	—	15	82
Herval based Ag NPs	Electrochemical	10–25	8.43	83
MS-Sp-P[5]-bodipy	Fluorimetry and colorimetry	1–150	0.06	37
MSp-P[5]-EN-B	Fluorimetry and colorimetry	1–100	0.33	43
MMIP	Fluorimetry	0–20	6.37	84
Gold nanoprobe	Colorimetry	5–100	5.0	85
PNBS–CQDs–Fe^{2+}	Fluorimetry	25–1500	5.0	86
MSp-TAB	Fluorimetry and colorimetry	5–100	2.72	Present work

TAB. To calculate the slope from the obtained data, the plots of fluorescence intensity ratio (I_0/I) at 523 nm *versus* Hg(II) concentration were used (Fig. S3†). The detection limit value for Hg(II) cation using **MSp-TAB** is 2.72 μM. In addition, the limit of detection (LOD) has been assessed in relation to sensors employing alternative methods and materials documented in previous studies (refer to Table 1). Compared to numerous prior studies, the magnetic fluorescent **MSp-TAB** hybrid exhibits notably low detection limits, suggesting its potential utility in detecting Hg(II) cations in water.

The reusability of the magnetic fluorescent **MSp-TAB** hybrid material was evaluated, and the obtained results (Fig. S4†) and their description are given in the ESI.†

3.2.4. Real sample analysis. The applicability of the prepared magnetic fluorescent **MSp-TAB** hybrid material was assessed using real samples. Tap water samples taken from 3 different points of the university were used without any processing. They were then analyzed by the addition of Hg(II) concentrations between 5 and 15 μM using the standard addition technique and the findings are presented in Table S1 in the ESI.† The recovery of added Hg(II) utilizing the magnetic fluorescent **MSp-TAB** hybrid material ranges from 94.00% to 99.40% (Table S1†). These findings indicate that the environmentally friendly magnetic fluorescent **MSp-TAB** hybrid material, employed for mercury(II) ion detection in samples, is dependable and viable.

4. Conclusions

Briefly, in this work, we have shown a simple and cost-effective synthesis strategy to synthesize magnetic fluorescence **MSp-TAB** hybrid material, and this strategy has demonstrated its potential to selectively and sensitively detect Hg(II) in aqueous media. FT-IR, SEM, EDX, XRD, and TGA were used to characterize the magnetic fluorescent **MSp-TAB** hybrid material. Excellent selectivity with a wide pH range and a response time of less than 30 minutes was demonstrated by studying the influence of diverse factors such as temperature, pH, and contact time on mercury(II) detection. **MSp-TAB** seems appropriate for detecting Hg(II) ions using the fluorometric method. This Hg(II) magnetic fluorescent hybrid material sensor achieved a LOD as low as 2.72 μM. It is believed that the prepared magnetic fluorescent **MSp-TAB** hybrid material will find great application in aqueous solutions and real environmental analysis, and we think that it will be an example for future research.

Data availability

Data are available upon request from the authors.

Author contributions

Melike Bayrak: conceptualization, methodology, investigation, visualization, synthesis of sensor material, application experiments, writing – original draft, synthesis of application experiments. Aysel Cimen: software, modelling review & editing, project administration, Ali Bilgic: supervision, conceptualization, writing – review & editing, synthesis of application experiments, instrumental resources.

Conflicts of interest

The authors declare that they do not have any known competing financial interests or personal relationships that might have influenced the findings reported in this paper.

Acknowledgements

The authors express their gratitude to the Scientific Research Project Commission of Karamanoğlu Mehmetbey University for their financial assistance (BAP-grant number 07-D-23). This manuscript constitutes a portion of Melike Bayrak's PhD thesis.

References

1 Z. Gul, S. Ullah, S. Khan, H. Ullah, M. U. Khan, M. Ullah, S. Ali and A. A. Altaf, *Crit. Rev. Anal. Chem.*, 2024, **54**, 44.
2 Q. Wu, H. Zhou, N. F. Tam, Y. Tian, Y. Tan, S. Zhou, Q. Li, Y. Chen and J. Y. Leung, *Mar. Pollut. Bull.*, 2016, **104**, 153.
3 E. Khan, *Int. J. Environ. Anal. Chem.*, 2023, **103**, 8890.
4 C. R. Thara and B. Mathew, *Talanta*, 2024, **268**, 125278.
5 S. Paz, C. Rubio, I. Frías, Á. J. Gutiérrez, D. González-Weller, V. Martín, C. Revert and A. Hardisson, *Chemosphere*, 2019, **218**, 879.
6 S. Patra, A. K. Golder and R. V. Uppaluri, *Results Opt.*, 2023, **11**, 100411.
7 C.-C. Bi, X.-X. Ke, X. Chen, R. Weerasooriya, Z.-Y. Hong, L.-C. Wang and Y.-C. Wu, *Anal. Chim. Acta*, 2020, **1100**, 31.
8 J. Yang, L. Feng, J. Liu, S. Li, N. Li and X. Zhang, *Sens. Actuators, B*, 2024, **398**, 134697.
9 M. Gochfeld, *Ecotoxicol. Environ. Saf.*, 2003, **56**, 174.
10 T. A. Saleh, G. Fadillah, E. Ciptawati and M. Khaled, *TrAC, Trends Anal. Chem.*, 2020, **132**, 116016.
11 L. Wang, D. Hou, Y. Cao, Y. S. Ok, F. M. Tack, J. Rinklebe and D. O'Connor, *Environ. Int.*, 2020, **134**, 105281.
12 N. C. Pomal, K. D. Bhatt, K. M. Modi, A. L. Desai, N. P. Patel, A. Kongor and V. Kolivoška, *J. Fluoresc.*, 2021, **31**, 635.
13 N. R. Jyothi and N. A. M. Farook, *Heavy Metal Toxicity in Public Health*, 2020, vol. 1.
14 S. Jimenez-Falcao, A. Villalonga, J. Parra-Nieto, A. Llopis-Lorente, P. Martinez-Ruiz, R. Martinez-Manez and R. Villalonga, *Microporous Mesoporous Mater.*, 2020, **297**, 110054.
15 V. Katseli, N. Thomaidis, A. Economou and C. Kokkinos, *Sens. Actuators, B*, 2020, **308**, 127715.
16 C. M. Carvalho, E.-H. Chew, S. I. Hashemy, J. Lu and A. Holmgren, *J. Biol. Chem.*, 2008, **283**, 11913.
17 T. W. Clarkson and L. Magos, *Crit. Rev. Toxicol.*, 2006, **36**, 609.
18 Y. Zhou, G. Chen, C. Ma, J. Gu, T. Yang, L. Li, H. Gao, Y. Xiong, C. Zhu and A. Hu, *Dyes Pigm.*, 2024, **222**, 111845.
19 F. Wang and J. Zhang, *Chin. Sci. Bull.*, 2013, **58**, 141.

20 E. Babaee, A. Barati, M. B. Gholivand, A. A. Taherpour, N. Zolfaghar and M. Shamsipur, *J. Hazard. Mater.*, 2019, **367**, 437.
21 B.-B. Wang, J.-C. Jin, Z.-Q. Xu, Z.-W. Jiang, X. Li, F.-L. Jiang and Y. Liu, *J. Colloid Interface Sci.*, 2019, **551**, 101.
22 F. Yan, D. Shi, T. Zheng, K. Yun, X. Zhou and L. Chen, *Sens. Actuators, B*, 2016, **224**, 926.
23 A. L. Squissato, D. P. Rocha, E. S. Almeida, E. M. Richter and R. A. Munoz, *Electroanalysis*, 2018, **30**, 20.
24 I. L. Almeida, M. D. Oliveira, J. B. Silva and N. M. Coelho, *Microchem. J.*, 2016, **124**, 326.
25 B. B. A. Francisco, A. A. Rocha, P. Grinberg, R. E. Sturgeon and R. J. Cassella, *J. Anal. At. Spectrom.*, 2016, **31**, 751.
26 Y. Li, Z. Zhu, H. Zheng, L. Jin and S. Hu, *J. Anal. At. Spectrom.*, 2016, **31**, 383.
27 J. Zhou, Y. Tian, X. Wu and X. Hou, *Microchem. J.*, 2017, **132**, 319.
28 Y. Xuan, X. Li, C. Yan and G. Wang, *Spectrochim. Acta, Part A*, 2023, **293**, 122479.
29 K. Leopold, M. Foulkes and P. Worsfold, *Anal. Chim. Acta*, 2010, **663**, 127.
30 G. Wang, Y. Lu, C. Yan and Y. Lu, *Sens. Actuators, B*, 2015, **211**, 1.
31 Z. Wang, Y. Zhang, J. Yin, Y. Yang, H. Luo, J. Song, X. Xu and S. Wang, *ACS Sustain. Chem. Eng.*, 2020, **8**, 12348.
32 M. L. Firdaus, A. Aprian, N. Meileza, M. Hitsmi, R. Elvia, L. Rahmidar and R. Khaydarov, *Chemosensors*, 2019, **7**, 25.
33 J. G. Kelly, F. X. Han, Y. Su, Y. Xia, V. Philips, Z. Shi, D. L. Monts, S. T. Pichardo and K. Xia, *Water, Air, Soil Pollut.*, 2012, **223**, 2361.
34 P. Ozmen, Z. Demir and B. Karagoz, *Eur. Polym. J.*, 2022, **162**, 110922.
35 N. Choudhury, M. Meghwal and K. Das, *Food Front.*, 2021, **2**, 426.
36 C.-C. Chang, S. Lin, S.-C. Wei, C.-Y. Chen and C.-W. Lin, *Biosens. Bioelectron.*, 2011, **30**, 235.
37 A. Bilgic and Z. Aydin, *J. Colloid Interface Sci.*, 2024, **657**, 102.
38 R. Thekkathu, D. Ashok, P. K. Ramkollath, S. Neelakandapillai, L. P. Kurishunkal, M. P. Yadav and N. Kalarikkal, *Chem. Phys. Lett.*, 2020, **742**, 137147.
39 Y. Gu, G. Meng, M. Wang, Q. Huang, C. Zhu and Z. Huang, *Sci. China Mater.*, 2015, **58**, 550.
40 S. Ali, M. Mansha, N. Baig and S. A. Khan, *Nanomaterials*, 2022, **12**, 1249.
41 P. A. Panchenko, A. V. Efremenko, A. S. Polyakova, A. V. Feofanov, M. A. Ustimova, Y. V. Fedorov and O. A. Fedorova, *Biosensors*, 2022, **12**, 770.
42 N. K. Choudhary, L. L. Mittapelli, P. K. Roy, G. Das, M. Mandal and K. R. Gore, *Spectrochim. Acta, Part A*, 2023, **285**, 121887.
43 A. Bilgic, A. Cimen, M. Bayrak and A. N. Kursunlu, *Mater. Today Sustain.*, 2024, **25**, 100696.
44 A. Bilgic, *J. Inst. Sci. Technol.*, 2022, **12**, 324.
45 A. Bilgic, *Colloids Surf., A*, 2021, **631**, 127658.
46 A. Bilgic, A. Cimen, E. Bastug and A. N. Kursunlu, *Chem. Eng. Res. Des.*, 2022, **178**, 61.
47 A. Bilgic, A. Cimen, A. N. Kursunlu and H. S. Karapınar, *Microporous Mesoporous Mater.*, 2022, **330**, 111600.
48 A. Çimen, A. Bilgiç, A. N. Kursunlu, İ. H. Gübbük and H. İ. Uçan, *Desalin. Water Treat.*, 2014, **52**, 4837.
49 Y. A. Maruthi and S. Ramakrishna, *Int. J. Biol. Macromol.*, 2022, **222**, 2957.
50 M. Lecoeuche, J. Borovička, A. K. Dyab and V. N. Paunov, *RSC Adv.*, 2024, **14**, 10280.
51 K. Yilmaz, I. H. Gubbuk and E. M. Cagil, *Macromol. Res.*, 2024, **32**, 45.
52 M. A. Kamboh, W. A. W. Ibrahim, H. R. Nodeh, M. M. Sanagi and S. T. H. Sherazi, *New J. Chem.*, 2016, **40**, 3130.
53 M. A. Kamboh, S. S. Arain, A. H. Jatoi, B. Sherino, T. S. Algarni, W. A. Al-Onazi, A. M. Al-Mohaimeed and S. Rezania, *Environ. Res.*, 2021, **201**, 111588.
54 Ü. Ecer, T. Şahan, A. Zengin and İ. H. Gubbuk, *Environ. Sci. Pollut. Res.*, 2022, **29**, 79375–79387.
55 N. Malhotra, J.-S. Lee, R. A. D. Liman, J. M. S. Ruallo, O. B. Villaflores, T.-R. Ger and C.-D. Hsiao, *Molecules*, 2020, **25**, 3159.
56 N. F. Ahmad, M. A. Kamboh, H. R. Nodeh, S. N. B. A. Halim and S. Mohamad, *Environ. Sci. Pollut. Res.*, 2017, **24**, 21846.
57 N. Mosleh, M. Najmi, E. Parandi, H. R. Nodeh, Y. Vasseghian and S. Rezania, *Chemosphere*, 2022, **300**, 134461.
58 M. Fayazi, D. Afzali, M. Taher, A. Mostafavi and V. Gupta, *J. Mol. Liq.*, 2015, **212**, 675.
59 J. M. Ageitos, S. Robla, L. Valverde-Fraga, M. Garcia-Fuentes and N. Csaba, *Polymers*, 2021, **13**, 2094.
60 A. K. Dyab, M. A. Mohamed, N. M. Meligi and S. K. Mohamed, *RSC Adv.*, 2018, **8**, 33432.
61 A. Bilgic, A. Cimen, M. Bayrak and A. N. Kursunlu, *Mater. Today Sustain.*, 2024, **25**, 100696.
62 A. N. Kursunlu and C. Baslak, *Tetrahedron Lett.*, 2018, **59**, 1958.
63 A. N. Kursunlu and E. Guler, *J. Lumin.*, 2014, **145**, 608.
64 A. Gul, M. Oguz, A. N. Kursunlu and M. Yilmaz, *Dyes Pigm.*, 2020, **176**, 108221.
65 H. Chen, Y. Li, S. Wang and Y. Zhou, *Appl. Surf. Sci.*, 2017, **402**, 384.
66 A. Bilgic, A. Cimen and A. N. Kursunlu, *Sci. Total Environ.*, 2022, **845**, 157170.
67 A. Bilgic, *J. Alloys Compd.*, 2022, **899**, 163360.
68 A. Bilgic, A. Cimen, M. Bayrak and A. N. Kursunlu, *J. Photochem. Photobiol., A*, 2024, **448**, 115346.
69 A. Bilgic, A. Cimen and A. N. Kursunlu, *Sci. Total Environ.*, 2023, **857**, 159312.
70 Ş. Yılmaz, A. Zengin, T. Şahan and İ. H. Gübbük, *J. Polym. Environ.*, 2023, **31**, 36.
71 A. M. Hassan, W. A. W. Ibrahim, M. B. Bakar, M. M. Sanagi, Z. A. Sutirman, H. R. Nodeh and M. A. Mokhter, *J. Environ. Manage.*, 2020, **253**, 109658.
72 A. K. Dyab, E. M. Abdallah, S. A. Ahmed and M. M. Rabee, *J. Encapsulation Adsorpt. Sci.*, 2016, **6**, 109.
73 S. F. F. S. Yaacob, N. S. A. Razak, T. T. Aun, S. K. M. Rozi, A. K. M. Jamil and S. Mohamad, *Ind. Crops Prod.*, 2018, **124**, 442.

74 J. Wang, S. Zheng, Y. Shao, J. Liu, Z. Xu and D. Zhu, *J. Colloid Interface Sci.*, 2010, **349**, 293.
75 N. Azmi, S. Ahmad and S. Low, *RSC Adv.*, 2018, **8**, 251.
76 D. Singhal, N. Gupta and A. K. Singh, *RSC Adv.*, 2015, **5**, 65731.
77 A. K. Manna, J. Mondal, R. Chandra, K. Rout and G. K. Patra, *J. Photochem. Photobiol., A*, 2018, **356**, 477.
78 C. Kaewprom, Y. Areerob, W.-C. Oh, K. L. Ameta and S. Chanthai, *Arab. J. Chem.*, 2020, **13**, 3714.
79 X. Zhang and Y.-Y. Zhu, *Sens. Actuators, B*, 2014, **202**, 609.
80 L. Li, B. Yu and T. You, *Biosens. Bioelectron.*, 2015, **74**, 263.
81 D. D. Yılmaz, D. A. Demirezen and H. Mıhçıokur, *Surf. Interfaces*, 2021, **22**, 100840.
82 N. Gupta, D. Singhal, A. K. Singh, N. Singh and U. Singh, *Spectrochim. Acta, Part A*, 2017, **176**, 38.
83 E. Eksin, A. Erdem, T. Fafal and B. Kıvçak, *Electroanalysis*, 2019, **31**, 1075.
84 S. Zhang, X. Wu, Q. Niu, Z. Guo, T. Li and H. Liu, *J. Lumin.*, 2017, **27**, 729.
85 S. He, D. Li, C. Zhu, S. Song, L. Wang, Y. Long and C. Fan, *Chem. Commun.*, 2008, 4885.
86 C. Karami, M. A. Taher and M. Shahlaei, *J. Mater. Sci.: Mater. Electron.*, 2020, **31**, 5975.